Programming Assignment

EE4595 Wavefield Imaging
Delft University of Technology

Burcu Erarslanoglu (5948355)
b.erarslanoglu@student.tudelft.nl

1 Introduction

Inverse scattering problems show their importance by determining the properties or the shape of an object. This takes place by analyzing how the object scatters known incident waves. The goal is to specifically deduce the internal characteristics of an object by observing the scattered wavefield outside the object. This is very useful in fields such as medical imaging, geophysical exploration, and radar detection. This report will present a two-dimensional inverse scattering problem, also called an inverse medium problem. Using multiple steps the image of an object will be reconstructed by solving the data equation with respect to the contrast function which is given by $\chi(\boldsymbol{\rho})$.

2 Methodology and Results

In this section, the solution steps in the report, for the reconstruction of $\chi(\boldsymbol{\rho})$, are carried out one by one. The methodology used and the results achieved are presented together.

Mathematical Formulation

For the problem, a two-dimensional homogeneous background configuration is considered that is characterized by a constant background wave speed c_b. The position vector of the point where the wavefield is being evaluated is given by $\boldsymbol{\rho} = x\mathbf{i}_x + y\mathbf{i}_y$. This wavefield is emitted by a line source with unit amplitude and it is located at a point with position vector $\boldsymbol{\rho}_s = x_s\mathbf{i}_x + y_s\mathbf{i}_y$. The field generated by this source satisfies the Helmholtz equation, which explains how a wave propagates in a medium with the following:

$$(\partial_x^2 + \partial_y^2 + k_b^2)\hat{u}_{\text{inc}} = -\delta(x - x_s)\delta(y - y_s), \tag{1}$$

where $k_b = \omega/c_b$ is the wave number of the background medium and the Delta functions on the right-hand side are Dirac distributions. The incident field, denoted by $\hat{u}^{inc}$ describes how the wave radiates from the line source and propagates through the medium. When the time convention is taken as $e^{j\omega t}$, the incident field radiating away from the line source is given by:

$$\hat{u}^{\text{inc}}(\boldsymbol{\rho}, j\omega) = -\frac{j}{4}H_0^{(2)}(k_b|\boldsymbol{\rho} - \boldsymbol{\rho}_s|). \tag{2}$$

In this equation, $H_0^{(2)}$ is the Hankel function of the second kind and order zero, k_b is the wave number of the background, $\boldsymbol{\rho}$ is the position vector, and $\boldsymbol{\rho}_s$ is the point where the position vector lies. The Hankel function $H_n^{(x)}(z)$ is a complex-valued solution to the Bessel differential equation, where $H_n^{(1)}(z)$ represents outgoing waves and $H_n^{(2)}(z)$ the incoming waves [1]. Because the problem at hand is radially symmetric in two dimensions, the order will be zero for the Hankel function. There is no angular dependency, thus it only varies with the distance from the source. Since the goal is to model the incident wavefield radiating away from the source, $H_0^{(2)}(z)$ is used as it describes waves moving towards the object domain $\mathbb{D}$.

Now, an object occupying the bounded domain $\mathbb{D}$ can be considered. Because the object is in the same field as the background field, its characteristics can be expressed as a contrast function incorporating the wave number of the background k_b and the position-dependent wave number of the object $k(\boldsymbol{\rho}) = \omega/c(\boldsymbol{\rho})$. The contrast function $\chi(\boldsymbol{\rho})$ characterizing the object is thus:

$$\chi(\boldsymbol{\rho}) = \left(\frac{k(\boldsymbol{\rho})}{k_b}\right)^2 - 1. \tag{3}$$

With the current two-dimensional configuration featuring an object domain $\mathbb{D}$, and a source at point $\boldsymbol{\rho}_s = (\lambda/2)\mathbf{i}_x + 10\lambda\mathbf{i}_y$, the Green's function can be written in a similar way as $\hat{u}_{\text{inc}}(\boldsymbol{\rho}, j\omega)$ with slight variations. The Green's function is given below:

$$\hat{G}(\boldsymbol{\rho} - \boldsymbol{\rho}', j\omega) = -\frac{j}{4} H_0^{(2)}(k_b|\boldsymbol{\rho} - \boldsymbol{\rho}'|) \tag{4}$$

Finally, in the Born approximation the scattered field at location $\boldsymbol{\rho} \notin \mathbb{D}$ is given as:

$$\hat{u}^{\text{sc}}(\boldsymbol{\rho}, j\omega) = -k_b^2 \int_{\boldsymbol{\rho}' \in \mathbb{D}} \hat{G}(\boldsymbol{\rho} - \boldsymbol{\rho}', j\omega)\chi(\boldsymbol{\rho}')\hat{u}^{\text{inc}}(\boldsymbol{\rho}', j\omega)\, dV. \tag{5}$$

Through Born approximation, the total field is approximated by the incident field inside the object/inversion domain. By examining eq. (5), the introduced terms of $\hat{u}^{\text{inc}}$ from eq. (2) and $\hat{G}$ from eq. (4) can be observed in the scattered field equation $\hat{u}^{\text{sc}}$. Substituting eq. (2) and eq. (4) in eq. (5) reveals:

$$\hat{u}^{\text{sc}}(\boldsymbol{\rho}, j\omega) = -k_b^2 \int_{\boldsymbol{\rho}' \in \mathbb{D}} \left(-\frac{j}{4} H_0^{(2)}(k_b|\boldsymbol{\rho} - \boldsymbol{\rho}'|)\right) \chi(\boldsymbol{\rho}') \left(-\frac{j}{4} H_0^{(2)}(k_b|\boldsymbol{\rho}' - \boldsymbol{\rho}_s|)\right) dV. \tag{6}$$

When eq. (6) is further simplified by using $j^2 = -1$, the following is obtained:

$$\hat{u}^{\text{sc}}(\boldsymbol{\rho}, j\omega) = \frac{k_b^2}{16} \int_{\boldsymbol{\rho}' \in \mathbb{D}} H_0^{(2)}(k_b|\boldsymbol{\rho} - \boldsymbol{\rho}'|)\chi(\boldsymbol{\rho}')H_0^{(2)}(k_b|\boldsymbol{\rho}' - \boldsymbol{\rho}_s|)dV. \tag{7}$$

Thus, eq. (7) represents the fully substituted form for the scattered field $\hat{u}^{\text{sc}}(\boldsymbol{\rho}, j\omega)$. The objective is to determine the contrast function $\chi(\boldsymbol{\rho})$ for points $\boldsymbol{\rho}$ within the domain $\mathbb{D}$, using the information provided by the found scattered field $\hat{u}^{\text{sc}}(\boldsymbol{\rho}, j\omega)$ at various receiver locations $\boldsymbol{\rho} = \boldsymbol{\rho}_m^R$ outside the domain $\mathbb{D}$, where $m = 1, 2, \ldots, M$.

Setup of the Cartesian Coordinate System and Source Configuration

In order to simplify the calculations, k_b is assumed to be 1. A Cartesian coordinate system where the x-axis is horizontal and points to the right, and the y-axis is vertical and points downward is considered. The object domain $\mathbb{D}$ is defined to be a square where the upper left corner is at the origin $(0, 0)$, and the lower right corner is at (λ, λ). Here, λ represents the wavelength of the background field and is given by $\lambda = 2\pi/k_b$. The source of the field is positioned at $\boldsymbol{\rho}_s = \left(\frac{\lambda}{2}\right)\mathbf{i}_x + 10\lambda\mathbf{i}_y$. This position vector places the source 1/2 wavelengths along the x-axis and 10 wavelengths down the y-axis. The sketch of this configuration is given in Figure 1 below:

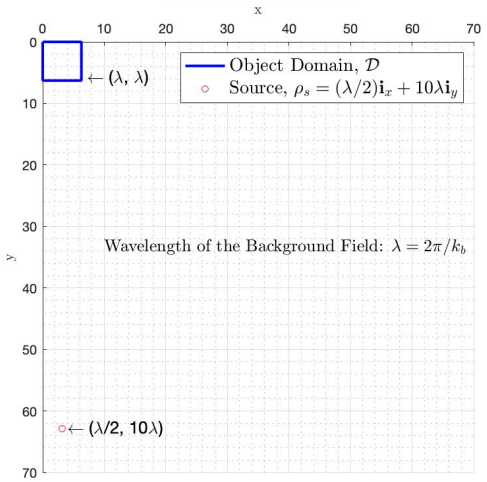

Figure 1: Sketch of the configuration for object domain $\mathbb{D}$ and source position $\boldsymbol{\rho}_s$ for $k_b = 1$.

The sketch in Figure 1 helps to visualize the problem setup. Within the object domain $\mathbb{D}$, a uniform grid with a step size of $h = \lambda/20$ is generated to discretize the 2D domain into square cells. This results in a total of $n = \lambda/h = \lambda/(\lambda/20) = 20$ grid points along each edge on the x-axis. Consequently, the total number of grid points covering the object domain $\mathbb{D}$ is $N = n \times n = 20 \times 20 = 400$. This result is verified using MATLAB as well.

Incident Field Calculation

In this part, the incident field $\hat{u}^{\text{inc}}(\boldsymbol{\rho}, j\omega)$ is found by directly using the eq. (2). It is worth noting that when the distance difference is calculated by $|\boldsymbol{\rho} - \boldsymbol{\rho}_s|$, position vector $\boldsymbol{\rho}$ is found according to the midpoint of a grid cell, which is given by:

$$\boldsymbol{\rho}_{ij} = x_i i_x + y_j i_y, \tag{8}$$

with

$$\begin{aligned} x_i &= \Delta x/2 + (i-1)\Delta x, \quad i = 1, 2 \ldots, m \\ y_j &= \Delta y/2 + (j-1)\Delta y, \quad j = 1, 2, \ldots, n. \end{aligned} \tag{9}$$

In eq. (9), Δx and Δy are the same as $h = \lambda/20$ defined earlier and m and n are equal to 20 which was found earlier. By using this information, the 2D images displaying the real and imaginary parts and the absolute value of $\hat{u}^{\text{inc}}(\boldsymbol{\rho}, j\omega)$ can be displayed as:

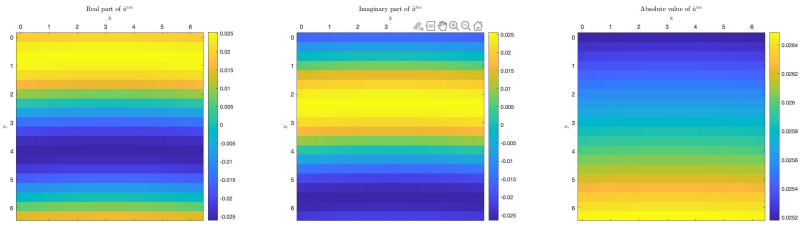

Figure 2: Real part, imaginary part and the absolute value of $\hat{u}^{\text{inc}}(\boldsymbol{\rho}, j\omega)$ for the configuration in Figure 1.

In Figure 2, it can be observed that there are 20 grids in both the vertical and horizontal directions, although the horizontal grids are not clearly visible. When the setup configuration is changed, the incident field experienced inside the object domain $\mathbb{D}$ also changes. There are a number of things that can be done for this purpose. The object domain $\mathbb{D}$'s location, source location $\boldsymbol{\rho}_s$, wavenumber $k_b = 1$ can be changed. In the following two Figures 3 and 4, the source position is moved closer to the object domain $\mathbb{D}$ and wavenumber $k_b = 1$ is changed to $k_b = 2$, respectively.

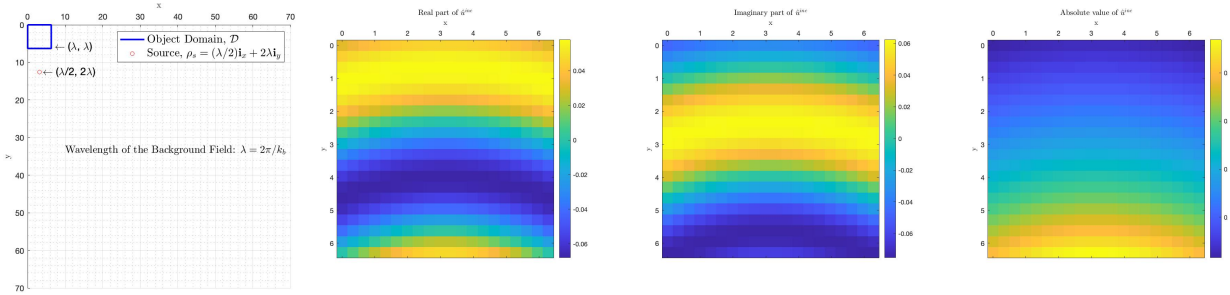

(a) Configuration. (b) Real part, imaginary part and the absolute value of $\hat{u}^{\text{inc}}(\boldsymbol{\rho}, j\omega)$.

Figure 3: Source position $\boldsymbol{\rho}_s$ moved closer to the object domain $\mathbb{D}$ for $k_b = 1$.

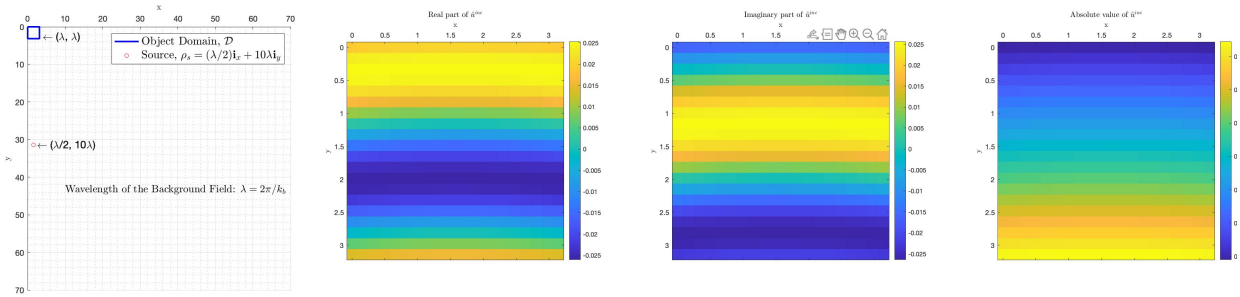

(a) Configuration. (b) Real part, imaginary part and the absolute value of $\hat{u}^{\text{inc}}(\boldsymbol{\rho}, j\omega)$.

Figure 4: Same source position $\boldsymbol{\rho}_s$ and object domain $\mathbb{D}$ for $k_b = 2$ instead of $k_b = 1$.

First of all, for the configuration in Figure 3a, the total number of grid points covering the object domain $\mathbb{D}$ is $N = 400$, since no change is done regarding the step size h. In Figure 4a, N remains 400 as well. Although the step size h changes due to the change in λ because of $k_b = 2$, this change reduces the object's edge length by half and its area by a factor of four, resulting in the same number of grid points.

When Figure 3b is observed the source's proximity is clearly visible in the field distribution. The incident field is blocky in the horizontal grids as well as the vertical grids. This is due to source position $\boldsymbol{\rho}_s$ being moved closer to the object domain $\mathbb{D}$ as waves start to exhibit more pronounced near-field characteristics. In far-field and in this 2D setting, the waves propagate in lines, which is clearly visible in Figure 2. If this problem setup were to have a 3D setting, the waves would propagate in wavefronts in far-field.

When analyzing Figure 4b for the incident field, it is observed that the real and imaginary parts, as well as the absolute value of $\hat{u}^{\text{inc}}(\boldsymbol{\rho}, j\omega)$, are identical to those presented in Figure 2. When $k_b = 2$, the configuration is scaled down by a factor of two, making the object domain $\mathbb{D}$ smaller and moving the source position $\boldsymbol{\rho}_s$ twice as close to $\mathbb{D}$. This setup maintains the same characteristics, with the wavelength of the background field being halved, resulting in no change in the incident field when compared to Figure 2.

For the next parts, the case where $\boldsymbol{\rho}_s = \left(\frac{\lambda}{2}\right)\mathbf{i}_x + 10\lambda\mathbf{i}_y$ and $k_b = 1$ is returned to.

Contrast Function

The contrast function $\chi(\boldsymbol{\rho}) \geq 0$ to be used in the rest of the report is given in Figure 5 below:

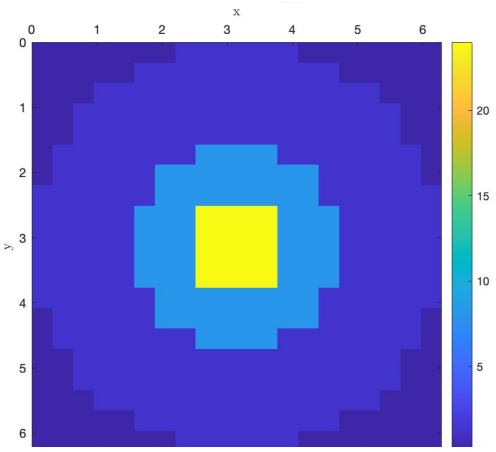

Figure 5: Contrast function $\chi(\boldsymbol{\rho})$.

The contrast function $\chi(\boldsymbol{\rho})$ more explicitly defined in eq. (3) is modeled to be real-valued because in most applications, the contrast function is indeed real-valued. For example, in medical imaging, contrast functions can quantify the difference between tissues in an MRI or CT scan, resulting in real values. This 2D image in Figure 5 is modeled as a 2D array in MATLAB.

Receiver Domain

In this part, the receiver domain $\mathbb{D}^{\text{rec}}$ is defined to be a line segment of length $L = 3\lambda$ with endpoints located at $(-\lambda, 1.5\lambda)$ and $(2\lambda, 1.5\lambda)$. On the receiver domain $\mathbb{D}^{\text{rec}}$, M receivers can be found which are essentially uniformly spaced grid points on the line segment. The receiver domain $\mathbb{D}_{\text{rec}}$ and its structure with M receivers can be found in Figures 6a and 6b below:

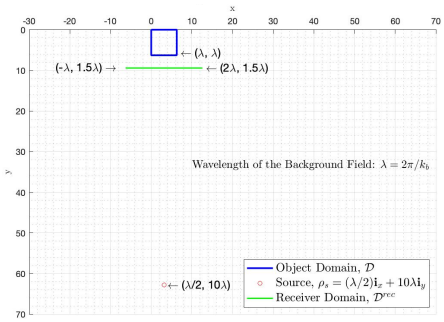

(a) Receiver domain $\mathbb{D}^{\text{rec}}$.

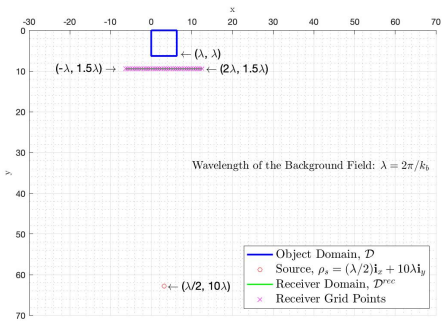

(b) Receiver domain $\mathbb{D}^{\text{rec}}$ ($M = 35$ receivers).

Figure 6: Sketch of the configuration with the receiver domain $\mathbb{D}^{\text{rec}}$ added.

The dependencies of the problem configuration on the parameter M will be further investigated in parts Singular Value Decomposition, Image Reconstruction and Analysis, and Noise Analysis parts.

Data Equation Discretization and System Matrix

The data equation modeling $\hat{u}^{\text{sc}}$ was provided in eq. (5). The integral can be approximated as a sum by using the composite midpoint rule. Discretizing the equation provides the benefit of converting the continuous problem into a discrete one, which can be efficiently solved using numerical methods. The approximation method to be used which is the composite midpoint rule approximates the integral by summing the function values at the midpoints of sub-intervals.

As discussed before, the object domain $\mathbb{D}$ was discretized into $n \times n$ grid points, the step size being $h = \lambda/20$. With this, each of the $N = 400$ grid cell has an area of h^2 and the midpoint of each grid cell is denoted by $\boldsymbol{\rho}_{ij}$ which was introduced in eq. (8) and eq. (9). Using the composite midpoint rule, the integral can be approximated as:

$$\hat{u}^{\text{sc}}(\boldsymbol{\rho}, j\omega) \approx -k_b^2 \sum_{i=1}^{n} \sum_{j=1}^{n} \hat{G}(\boldsymbol{\rho} - \boldsymbol{\rho}_{ij}, j\omega)\chi(\boldsymbol{\rho}_{ij})\hat{u}^{\text{inc}}(\boldsymbol{\rho}_{ij}, j\omega)(h)^2 \tag{10}$$

This formula in eq. (10) approximates the integral by summing the contributions from each grid cell, weighted by the value of the integrand at the cell midpoints and the cell area.

To exploit this structure further the Green's function $\hat{G}(\boldsymbol{\rho}-\boldsymbol{\rho}_{ij}, j\omega)$, the contrast function $\chi(\boldsymbol{\rho}_{ij})$, and the incident field $\hat{u}^{\text{inc}}(\boldsymbol{\rho}_{ij}, j\omega)$ can all be described as column vectors $\hat{\mathbf{G}} \in \mathbb{C}^{N\times 1}$, $\mathbf{x} \in \mathbb{C}^{N\times 1}$ and $\hat{\mathbf{u}}^{\text{inc}} \in \mathbb{C}^{N\times 1}$ with $N = 400$. Note that, with the formulation, $\hat{\mathbf{u}}^{\text{sc}}(\boldsymbol{\rho}, j\omega)$ also becomes a column vector in $\mathbb{C}^{N\times 1}$. This simplifies the coding done in MATLAB as well, where the matrices are vectorized using the `reshape()` command.

Next, the system matrix $\mathbf{A} \in \mathbb{C}^{M \times N}$ can be generated using this formulation of the discretized data equation. In this context, M represents the number of receiver points. Each row of N corresponds to one of these M receiver points.

Singular Value Decomposition

Singular Value Decomposition (SVD) is a fundamental matrix factorization technique which decomposes a given matrix into three simpler matrices, revealing many useful properties. This full decomposition can be carried out for the system matrix $\mathbf{A}$ which is defined as:

$$\mathbf{A} = \mathbf{U}\mathbf{S}\mathbf{V}^H = \begin{bmatrix} \mathbf{U}_R & \mathbf{U}_0 \end{bmatrix} \begin{bmatrix} \mathbf{S}_R & 0 \\ 0 & 0 \end{bmatrix} \begin{bmatrix} \mathbf{V}_R & \mathbf{V}_0 \end{bmatrix}^H \tag{11}$$

where $\mathbf{U}$ and $\mathbf{V}$ are the left and right singular matrices of $\mathbf{A}$, respectively. Left singular vector matrix $\mathbf{U}$ is unitary and $M \times M$, right singular vector matrix $\mathbf{V}$ is unitary and $N \times N$. $\mathbf{S}$ is a diagonal matrix having size $M \times N$ containing the singular values σ_i on the diagonal, which are arranged in ascending order.

As it can be seen in the full SVD decomposition in eq. (11), $\mathbf{S}$ has the structure diag $(\sigma_1, \sigma_2, \ldots, \sigma_R, \sigma_{R+1}, \ldots, \sigma_N$ and $\sigma_1 \geqslant \sigma_2 \geqslant \ldots \geqslant \sigma_R > 0 = \sigma_{R+1} = \ldots = \sigma_N$. The structure of $\mathbf{S}$in this problem setting is slightly different than what is described above in eq. (11), and its implications are very important. when $M > N$ and $N > M$ will now be described. If $M > N$, the system is said to be overdetermined and $\mathbf{S}$ therefore has the structure:

$$\mathbf{S} = \begin{bmatrix} \mathbf{S}_R \\ 0 \end{bmatrix}. \tag{12}$$

On the other hand, for $N > M$, the system is underdetermined and $\mathbf{S}$ is given by:

$$\mathbf{S} = \begin{bmatrix} \mathbf{S}_R & 0 \end{bmatrix}. \tag{13}$$

From Figure 6b, $M = 35$ and $N = 400$, therefore the system at hand is an underdetermined one, having the structure in eq. (13).

The SVD gives the directions (singular vectors) along which the data has the most significant variations, which is indicated by the value of the singular value σ_i. Thus, the first columns of $\mathbf{U}$ and $\mathbf{V}$ will correspond to the direction containing the most important information. When σ_i is low, its corresponding singular vectors will most likely correspond to noise. For different numbers of receivers M, the singular values σ_i where $i = 1, ..., M$ reveal important characteristics about the system, which can be analyzed in Figure 7 below:

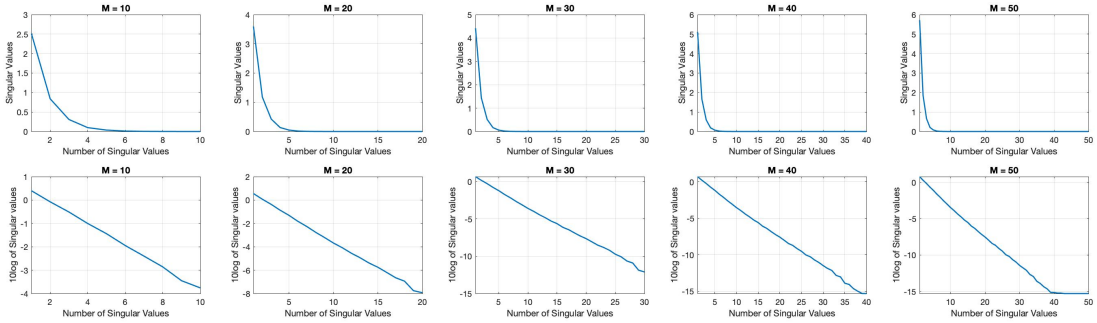

Figure 7: Singular values for different M presented in both regularly and in $\log_{10}$ scale.

In Figure 7, a rapid initial decay of singular values in all cases can be seen. This suggests that the first few singular vectors capture the most significant variations in the data. The plots in both formats provide complementary results; however, $\log_{10}$ is particularly useful for understanding the contribution of smaller singular values. As M increases, the number of singular values and the decay rate increases, particularly after $M = 50$.

Scattered Field Calculation

The computation of the scattered field $\hat{\mathbf{u}}^{\text{sc}}$ as a column vector occupying $\mathbb{C}^{M\times 1}$, is quite straightforward with the following calculation:

$$\hat{\mathbf{u}}^{\text{sc}} = \mathbf{A}\mathbf{x}, \tag{14}$$

where $\mathbf{A}$ corresponds to the system matrix of size $M \times N$ and $\mathbf{x}$ of size $N \times 1$ corresponds to the vectorized contrast function $\chi(\boldsymbol{\rho})$.

Image Reconstruction and Analysis

Since the system matrix $\mathbf{A}$ has been constructed, the next step is to solve for the earlier defined contrast function $\mathbf{x}$. The linear system was described in eq. (14). One might think that this problem has a simple solution with $\mathbf{x} = \mathbf{A}^{-1}\hat{\mathbf{u}}^{\text{sc}}$; however, this does not hold since $\mathbf{A}$ is not invertible because $M \neq N$. Even in the case that $\mathbf{A}$ is square, it is singular so inversion is still not possible. To remedy this and to find $\mathbf{x}$, two methods based on minimum norm solution will be discussed. These are the SVD-based and Moore-Penrose pseudoinverse-based approaches.

For the SVD based approach, the thin or in other words the reduced SVD is used. Note that, due to the problem setup with M number of receivers and N grid points; $\mathbf{S}$ expression becomes the one described in eq. (13). The reduced SVD is hence written as follows:

$$\mathbf{A}_R = \mathbf{U}_R\mathbf{S}_R\mathbf{V}_R^H \tag{15}$$

When the inverse of this decomposition is taken, $\mathbf{A}_R^{-1} = \mathbf{V}_R\mathbf{S}_R^{-1}\mathbf{U}_R^H$ is obtained by exploiting the unitary matrix properties. Then, the linear system can be solved as follows:

$$\mathbf{x}_{\text{mn}} = \mathbf{V}_R\ \mathbf{S}_R^{-1}\mathbf{U}_R^H\hat{\mathbf{u}}^{\text{sc}} \tag{16}$$

This concludes the SVD-based approach using minimum norm solution.

The pseudoinverse method provides a straightforward approach for solving the linear system in eq. (14). It uses $\mathbf{A}^\dagger$ to find the least-squares solution as follows:

$$\mathbf{x}_{\text{mn}} = \mathbf{A}^\dagger\hat{\mathbf{u}}^{\text{sc}}. \tag{17}$$

However, the expansion of $\mathbf{A}^\dagger$ changes when the system is overdetermined or underdetermined. For the overdetermined system of full rank, the minimum norm solution is given as:

$$\mathbf{x}_{\text{mn}} = \mathbf{A}^H\left(\mathbf{A}\mathbf{A}^H\right)^{-1}\hat{\mathbf{u}}^{\text{sc}}, \tag{18}$$

and for the underdetermined system of full rank, the solution is given as:

$$\mathbf{x}_{\text{mn}} = \left(\mathbf{A}^H\mathbf{A}\right)^{-1}\mathbf{A}^H\hat{\mathbf{u}}^{\text{sc}}. \tag{19}$$

The eq. (19) is the form that is used for this problem and this concludes the pseudo-inverse-based approach. This approach can be easily followed in MATLAB by using the `pinv()` command. The last step before seeing the reconstructions is reshaping the solution vector $\mathbf{x}_{mm}$ into a 2D array.

Below, the reconstruction results for the SVD and pseudo-inverse-based approach can be seen:

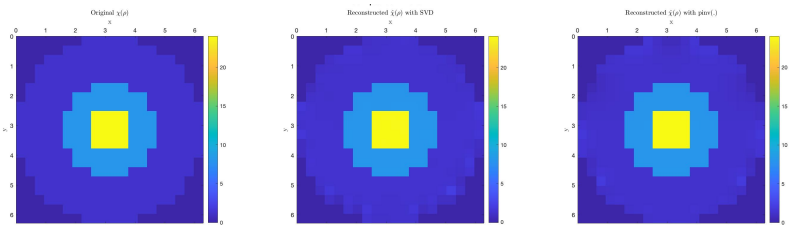

Figure 8: Contrast function $\chi(\boldsymbol{\rho})$, reconstructed contrast functions $\hat{\chi}(\boldsymbol{\rho})$ with SVD and `pinv(.)`.

From Figure 8 it is seen that the reconstructions with both the SVD and `pinv(.)` method are effective in reconstructing the contrast function with the configuration in Figure6. To see which method performs better, mean square error (MSE) and mean absolute error (MAE) metrics can be found. The results for these error metrics are given in Table 1 below:

Table 1: Error metrics for SVD and `pinv(.)` reconstructions.

	SVD	`pinv(.)`
MSE	0.013016	0.016794
MAE	0.061445	0.068034

As it can be seen, for both the MSE and MAE the error attained with the SVD approach is less than that of the `pinv()` approach. Therefore, for the rest of the report, the SVD-based minimum norm reconstruction will be used.

The images in Figure 8 are obtained by using the real part of the reconstructions since the original contrast function was real-valued. However, because the scattered field was complex-valued the reconstructed contrast functions were complex-valued as well. To see what was reconstructed exactly, imaginary part and absolute value of the reconstructions can be seen in Figure 9 below:

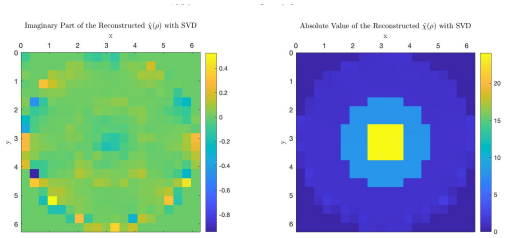

Figure 9: Imaginary part and absolute value of the reconstructed contrast function $\hat{\chi}(\boldsymbol{\rho})$ with SVD.

As it can be seen on the left subplot of Figure 9, the reconstructed imaginary values are very small, this means that the reconstructions were successful since the original contrast funtion were real-valued. When the right subplot is observed, it is seen that the absolute value of the reconstruction is very similar to the original contrast function. This is expected due to the small contribution of the imaginary values on the reconstruction.

Now, the effect of number of receivers M on the reconstruction results can be observed. For this purpose, only SVD is used since it yielded better results in Table 1. The Figure 10 below displays the reconstruction results for different M:

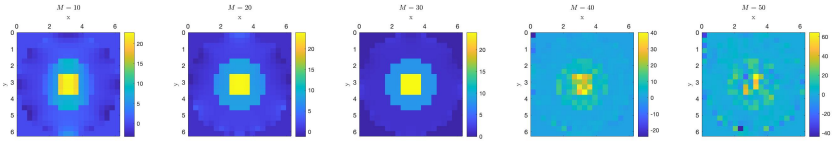

Figure 10: Reconstructed contrast functions $\hat{\chi}(\boldsymbol{\rho})$ with SVD for different number of receivers M.

As seen above, and also Figure 8, the reconstruction error is the least when the number of receivers M is between 25 and 35. Of course, this varies with the setup and chosen contrast function.

Noise Analysis

The final part concerns the effect of noise on the reconstructions for the inverse scattering problem. To investigate this, complex noise is added to the scattered field which is also complex-valued. The sketch of the configuration with its respective reconstruction of the contrast function can be viewed in Figure 11 below:

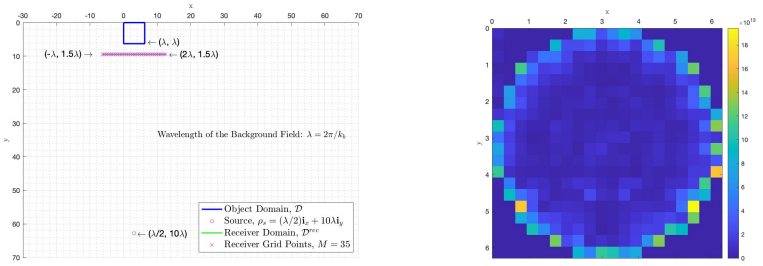

(a) Original configuration. (b) $\hat{\chi}(\boldsymbol{\rho})$ with SVD.

Figure 11: Reconstruction results for the original configuration under noise. Noise level equals 1.

As can be seen, the reconstruction performance is very poor. This is due the matrix $\mathbf{A}$ being ill-conditioned. The condition number is used measure how sensitive a function is to changes or errors in the input. Since $\mathbf{A}$ has a high condition number of 8.724867e+14, even very small noises result in a poor reconstruction. To tackle this extreme sensitivity to noise, the problem setup can be changed by changing the source and receiver locations, number of receivers used and the frequency of system by changing wave number k_b. Also, because the added noise is very large compared to the values in the scattered field, an appropriate noise level can be considered. Figures below feature the sketch of the configuration with its respective reconstruction of the contrast function:

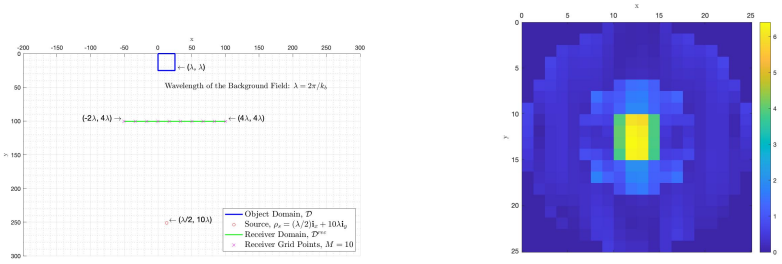

(a) Changed configuration. (b) $\hat{\chi}(\boldsymbol{\rho})$ with SVD.

Figure 12: Reconstruction results for the changed configuration under noise. Changes made: $k_b = 0.25$, received domain elongated and $M = 10$ receivers used. Noise level equals 0.001.

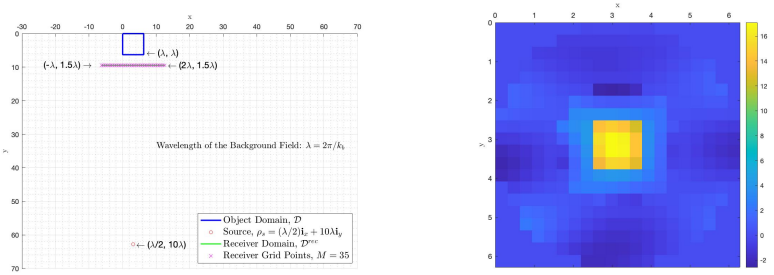

(a) Original configuration. (b) $\hat{\chi}(\boldsymbol{\rho})$ with SVD, regularized.

Figure 13: Reconstruction results using Tikhonov regularization. Noise level equals 1, $\lambda = 0.01$.

In both Figures 12b and 13b, the results achieved are much better than the one in Figure 11b. In Figure 12, the wave number k_b is reduced, making the object domain $\mathbb{D}$ larger, but this scales the problem setup bigger. Because decreasing k_b means using waves with longer wavelengths, this might reduce the resolution but it can make the system less sensitive to noise. Since the contrast function does not require much resolution, decreasing k_b does not have adverse effects. Next, the receiver domain $\mathbb{D}^{\text{rec}}$ is elongated, and $M = 10$ receivers are used. This makes the receivers less susceptible to noise and interference. One drawback of using a reduced number of receivers is reduced spatial resolution. Still, these changes were not enough and the noise level that scales the noise was chosen as 0.001. In Figure 13, the reconstruction with the Tikhonov regularization term was given. This is especially significant since the noise level was 1. This method stabilizes the solution of a linear system affected by noise, using a regularization parameter λ to balance between fitting the data and smoothing the solution, achieving improved results.

3 Conclusion

In this report, an inverse scattering problem was solved to find the contrast function for different problem setups under noiseless and noisy scenarios for an underdetermined system. Born approximation was used to linearize the problem. The results achieved showed that when there was no noise, the reconstructions were near perfect. However, when noise was added to the system the reconstruction performance degraded significantly. To remedy this, different setup configurations and Tikhonov regularization were tried, delivering improved results. Given the nature of the problem, there is a lot of room for improvement and future work. Future work can focus on several key areas to enhance the robustness and accuracy of the inverse scattering problem solutions under noisy conditions. By incorporating signal processing methods such as wavelet denoising or deep learning-based noise suppression, the quality of the reconstructed images can be significantly improved. Furthermore, expanding the problem setup configurations further can also provide valuable insights and enhance the overall reconstruction quality and robustness against noise. In this regard, a multi-frequency data could be used. The MATLAB code can be found in [2].

References

[1] MATLAB, *Hankel function*, https://www.mathworks.com/help/matlab/ref/besselh.html, 2024.

[2] Burcu Erarslanoglu, *Code*, https://github.com/burcuerarslanoglu/Wavefield-Imaging, 2024.